Supplementary Information (SI) for:

Thermogalvanic bricks: Optimising large dimension thermocells for air and water valorisation

Rebecca Haughton-James,[a,†] Sireenya Mesawang,[a,†] Mark A. Buckingham,[a,b] Robert Taylor,[c] Patrick E. Phelan[d] and Leigh Aldous[a,e*]

[a] Department of Chemistry, King's College London, London, UK

[b] Department of Materials, The University of Manchester, Manchester, UK

[c] Mechanical and Manufacturing Engineering, UNSW Sydney, Sydney, Australia

[d] School for Engineering of Matter, Transport and Energy, Arizona State University, Tempe, USA

[e] Department of Chemical Engineering, National Taiwan University, Taipei, Taiwan

† Students contributed equally to this work

* Corresponding Author: leighaldous@ntu.edu.tw

Table of Contents

Experimental, Exemplar Raw Data and Tabulated Results

S1. Relevant thermogalvanic equations

In a thermogalvanic cell, two electrodes share a redox couple with both redox states present. When the electrodes are at a dissimilar temperature (ΔT), a potential difference (ΔV) can typically be measured. This gives rise to the thermogalvanic Seebeck coefficient, S_e, where, in the absence of temperature-dependent chemical equilibria, it has the relationship shown in equation (1). The S_e is also directly correlated to the entropy difference between the redox states of the redox couple, ΔS_{rc};

$$S_e = \frac{\Delta V}{\Delta T} = \frac{\Delta S_{rc}}{nF} \tag{1}$$

This potential difference, ΔV, can be seen as the driving force (or overpotential) that can result in a flow of current being generated. It has previously been experimentally demonstrated that this relationship can be modelled using a modified Butler-Volmer equation.[1] The standard Butler-Volmer equation is;

$$j_{sc} = Fk^0\left(C_{ox}^{\alpha_a} C_{red}^{\alpha_c}\right) \cdot \left\{exp\left[\frac{\alpha_a nF\eta}{RT}\right] - exp\left[-\frac{\alpha_c nF\eta}{RT}\right]\right\} \tag{2}$$

If we consider $[Fe(CN)_6]^{3-} + e^- \rightarrow [Fe(CN)_6]^{4-}$ in a thermogalvanic cell then (i) $n = 1$ and (ii) the overpotential, η, can be replaced with $\eta = 0.5\, V_{OCP}$. Additionally (iii) the current at the hot side can be considered as limited by the current available at the cold side (for $[Fe(CN)_6]^{3-/4-}$, it is the cathodic process occurring at T_{cold}), allowing us to modify the equation to;

$$j_{sc} = Fk^0\left(C_{ox}^{\alpha_a} C_{red}^{\alpha_c}\right) \cdot \left\{exp\left[\frac{0.5V_{ocp}\alpha_c F}{RT_{cold}}\right] - exp\left[-\frac{0.5V_{ocp}\alpha_c F}{RT_{cold}}\right]\right\} \tag{3}$$

Furthermore, if we assume $\alpha_a + \alpha_c = 1$, and $\alpha_a \approx \alpha_c \approx 0.5$, and if we deliberately use $C_{ox} = C_{red}$ then both can be replaced with the same variable, C, such that $C_{ox}^{\alpha_a} C_{red}^{\alpha_c} = C^{0.5} C^{0.5} = C$. Applying these to the equation, we obtain;

$$j_{sc} = Fk^0C \cdot \left\{ exp\left[\frac{0.25V_{ocp}F}{RT_{cold}}\right] - exp\left[-\frac{0.25V_{ocp}F}{RT_{cold}}\right]\right\} \quad (4)$$

Typically, thermogalvanic cells in steady-state discharge conditions are mass transport limited, or a combination of kinetic and mass transport limited. There is therefore a number of in-series or parallel resistances (or kinetic factors) to be considered, and these can replace k^0 as an aggregated kinetic function, k_{agg}. Assuming FC is a constant, we obtain;

$$j_{sc} = constant \cdot k_{agg}\left\{ exp\left[\frac{0.25V_{ocp}F}{RT_{cold}}\right] - exp\left[-\frac{0.25V_{ocp}F}{RT_{cold}}\right]\right\} \quad (5)$$

If the S_e is taken as -1.44 mV K^{-1} for $[Fe(CN)_6]^{3-} + e^- \rightarrow [Fe(CN)_6]^{4-}$ and a moderate temperature difference is applied (*e.g.* ΔT = 20 K, T_{cold} = 293 K), then V_{ocp} should be *ca.* -28.8 mV. This means the $\left\{ exp\left[\frac{0.25V_{ocp}F}{RT_{cold}}\right] - exp\left[-\frac{0.25V_{ocp}F}{RT_{cold}}\right]\right\}$ components can be calculated as {0.75 – 1.33} or -0.58, *e.g.* a negative j_{sc} is expected, but the reaction is not significantly in the forward direction. Therefore, both exponential functions need to be retained, but to further simplify we can apply the hyperbolic *sinh* function, such that

$$j_{sc} = constant \cdot k_{agg} \cdot 2sinh\left[\frac{0.25V_{ocp}F}{RT_{cold}}\right] \quad (6)$$

Next, it is well established that the maximum power, P_{max}, is typically observed at half the maximum current density, j_{sc}, and half the V_{ocp}, such that $P_{max} = 0.25V_{ocp}j_{sc}$. Substituting this in we come to;

$$P_{max} = 0.25V_{ocp}j_{sc} = 0.25V_{ocp} \cdot constant \cdot k_{agg} \cdot 2sinh\left[\frac{0.25V_{ocp}F}{RT_{cold}}\right] \quad (7)$$

The V_{ocp} is a constant in an experiment given by $V_{ocp} = \Delta T\Delta S_{rc}/nF$. Taking n = 1 and replacing V_{ocp} we obtain the below equation;

$$P_{max} = 0.25\frac{\Delta T\Delta S_{rc}}{F} \cdot constant \cdot k_{agg} \cdot 2sinh\left[\frac{0.25\Delta T\Delta S_{rc}}{RT_{cold}}\right] \quad (8)$$

Combining the various constants (*constant*, 0.25, ΔS_{rc}, *F*, 2) into the aggregate *'constant$_1$'* component, and inside the *sinh* function we combine 0.25, ΔS_{rc} and *R* to '*constant*$_2$', we simplify to the below equation, where remaining variables are indicated in red;

$$P_{max} = constant_1 \cdot k_{agg} \cdot \Delta T \cdot sinh\left[constant_2 \frac{\Delta T}{T_{cold}}\right] \tag{9}$$

Given that $\Delta T = T_{hot} - T_{cold}$, it stands that

$$P_{max} = constant_1 \cdot k_{agg} \cdot (T_{hot} - T_{cold}) \cdot sinh\left[constant_2 \frac{T_{hot} - T_{cold}}{T_{cold}}\right] \tag{10}$$

Expressing (9) and (10) as proportional relationships by removing *constant*$_1$, we obtain;

$$P_{max} \propto k_{agg} \cdot (\Delta T) \cdot sinh\left[constant_2 \frac{\Delta T}{T_{cold}}\right] \tag{11}$$

$$P_{max} \propto k_{agg} \cdot (T_{hot} - T_{cold}) \cdot sinh\left[constant_2 \frac{T_{hot} - T_{cold}}{T_{cold}}\right] \tag{12}$$

Finally, we can see that if our applied ΔT is only *ca.* 20 K, but T_{cold} is significantly larger (293 K), then $(T_{hot} - T_{cold})/T_{cold}$ is significantly smaller than 1, *e.g.* (313 K – 293 K)/(293 K) = 0.068. The aggregate constant, *constant*$_2$, representing $0.25\Delta S_{rc}/R$ is given by (0.25 × 95.4 J K^{-1} mol^{-1}) / (8.314 J K^{-1} mol^{-1}) = 2.87 (NB: ΔS_{rc} taken from reference [2]), such that overall *sinh*(0.20). Applying *sinh*(x) ≈ x for x < 1 (NB: this is no longer quantitative but does show simplified semi-quantitative relationships) we can re-express equation (12) as

$$P_{max} \propto constant_2 \cdot k_{agg} \cdot (T_{hot} - T_{cold}) \frac{(T_{hot} - T_{cold})}{T_{cold}} \tag{13}$$

And can further simplify to

$$P_{max} \propto k_{agg} \cdot \frac{(T_{hot} - T_{cold})^2}{T_{cold}} \tag{14}$$

We can see here that the maximum power generated, P_{max}, by the thermogalvanic cell is (a) influenced by both the temperature difference (ΔT) and the absolute temperature of the T_{hot} and T_{cold}, and (b) also influenced by k_{agg}; if we assume kinetic electron transfer rates (k^0) remain unchanged, then *via* the mass transport component in k_{agg} the power is directly proportional to the kinetic rate of mass transfer (or, P_{max} is decreased if mass transport resistance, R_{mt}, increases).

These equations help explain why, in this work, as the experienced ΔT value increases, the P_{max} increases significantly. If *e.g.* adding gelling agent frustrates mass transport, it will typically frustrate both heat flux and redox couple mass transport,[3] thus increasing ΔT and decreasing k_{agg}. At this stage P_{max} increases due to the greater significance of ΔT ($P_{max} \propto \Delta T^2/T_{cold}$) compared to k_{agg} ($P_{max} \propto k_{agg}$, or $P_{max} \propto 1/R_{mt}$). Once the electrolyte is sufficiently thermally resistive such that the experienced applied ΔT value now matches the applied ΔT, at this stage ΔT becomes a constant. Further changes in the system (*e.g.* going beyond 1.5 or 2.5 wt/v% sodium poly(acrylate) in this study) no longer influences ΔT but does decrease k_{agg}, thus resulting in a decrease in P_{max} as more gelling agent is added.

S2. Electrolyte and gelation

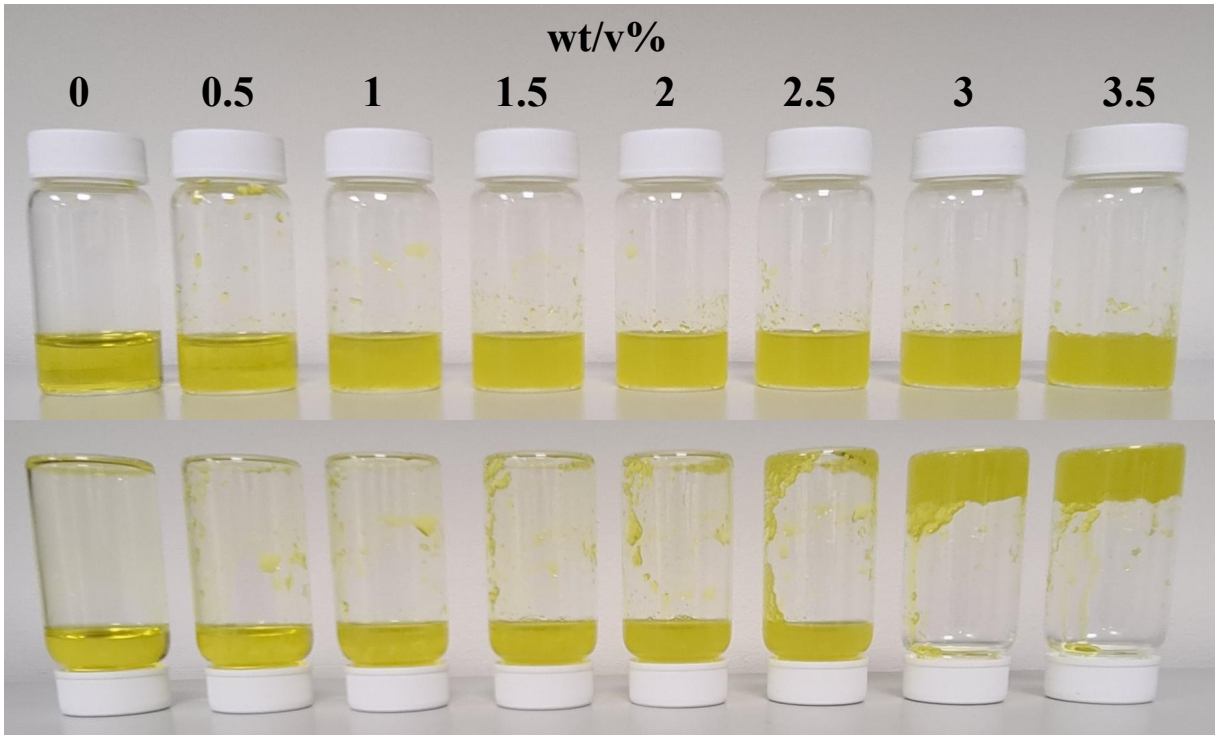

Figure S1. Photographs of solutions of 0.2 M $K_3[Fe(CN)_6]$, 0.2 M $K_4[Fe(CN)_6]$ and 0.05 M K_2CO_3, as a function of the amount of wt/v% sodium poly(acrylate) gelling agent straight. The solutions were allowed to gel for 5 minutes, and (top) had their photograph taken and (bottom) were then inverted and left for a further 5 minutes

S3. Thermogalvanic bricks

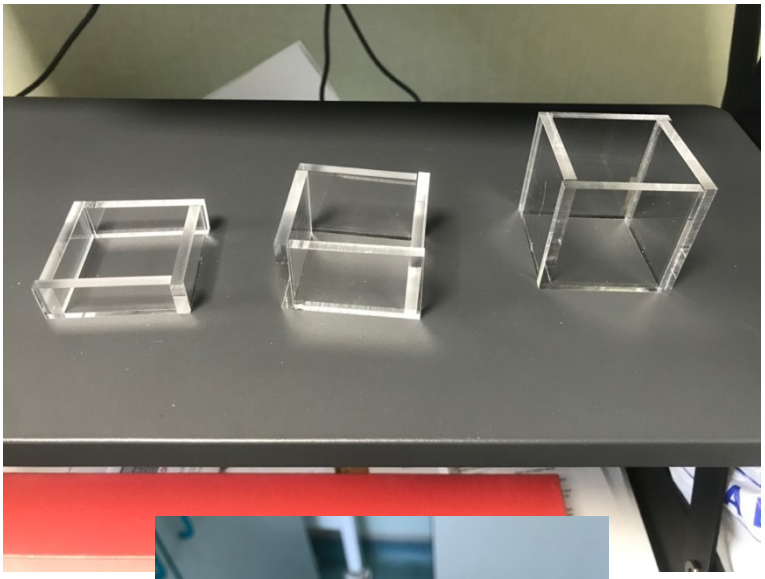

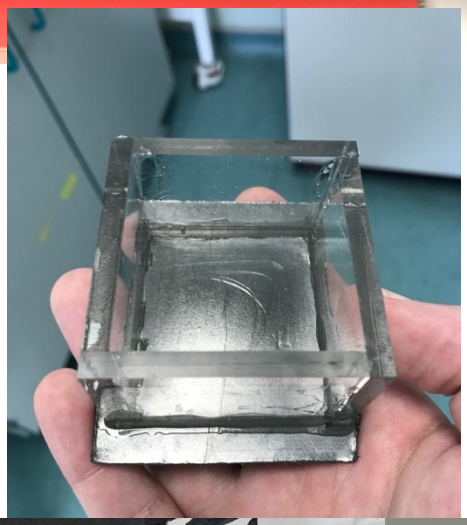

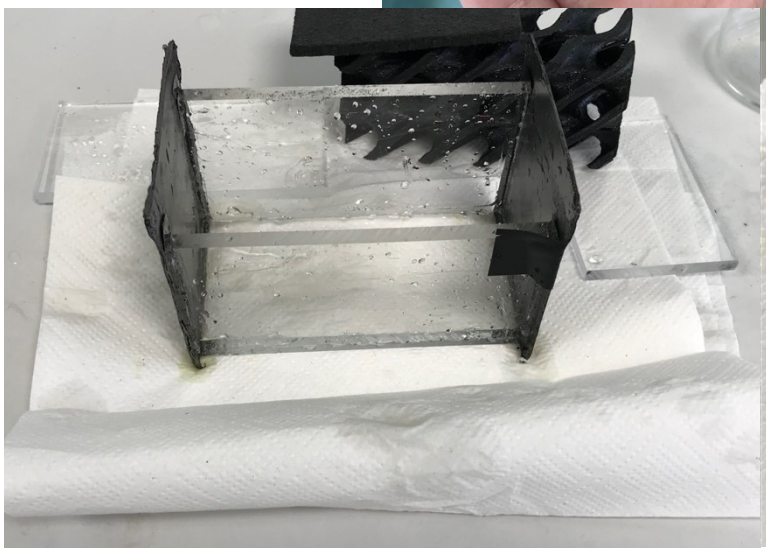

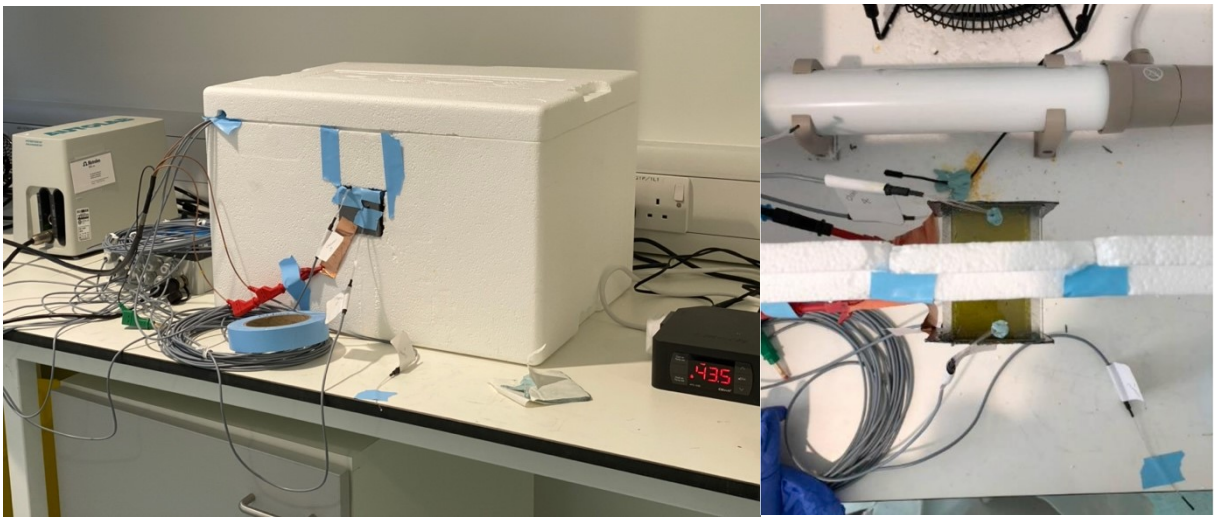

Figure S2. Photos of (top left) the 25, 50, and 75 mm cells prior to construction, (top right) the 50 mm cell with one electrode adhered; (centre left) the 100 mm cell after being washed before re-use; (centre right) the 25 mm cell in the insulated box wall; (bottom left) the 50 mm cell being measured; and (bottom right) a cross-section view of the 75 mm cell (NB: the optimised arrangement of components, including dimensions, are summarised in the text).

Table S1. Summarising the theoretical volume (for the 45 mm × 45 mm by width internal area of the cells), the amount that was used to achieve reproducible electrode contact surface areas without overfilling the cell, and the resulting geometric surface area of each graphite electrode in contact with the electrolyte.

Cell width / mm	**Theoretical volume / mL**	**Added volume of electrolyte / mL**	**Geometric surface area of graphite electrodes in contact with electrolyte / cm^2**
25	51	43	17.1
50	101	90	16.0
75	152	120	16.5
100	203	174	16.3

S4. Thermoelectrochemical setup using the water-water temperature-controlled apparatus

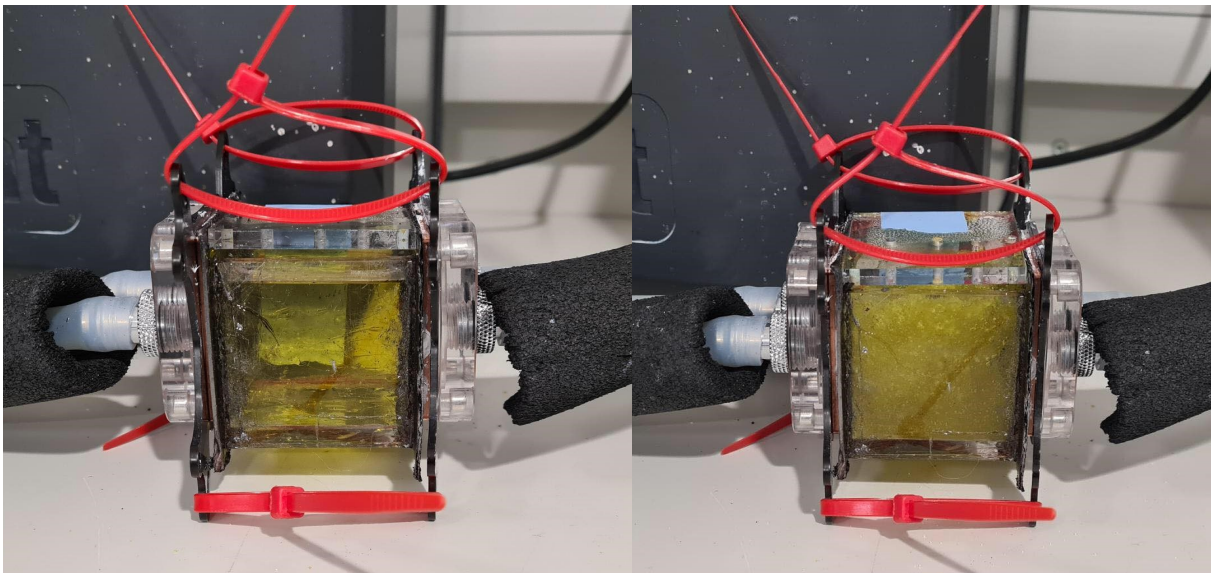

Figure S3. Photographs of the 50 mm thermocell filled with (left) liquid electrolyte and (right) 3 wt/v% gelled electrolyte, set up with the water-heating and water-cooling apparatus.

S5. Exemplar data for thermogalvanic properties of air-air apparatus

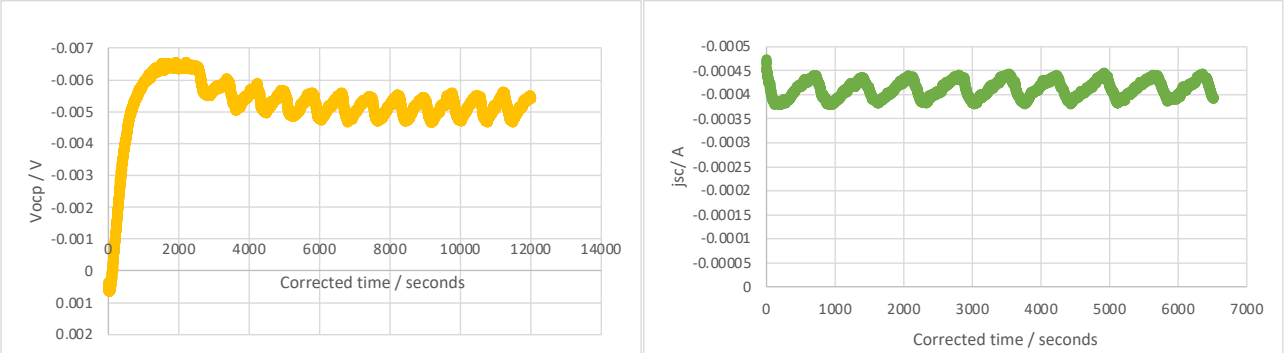

Figure S4. Exemplar raw data measured for the 75 mm thermocell (air-air set up, 0 wt% gel) showing (left) V_{ocp} measurement and (right) j_{sc} measurement. The oscillating data represents the heater switching off and on due to the hysteresis in the temperature control unit but was readily removed by averaging the data. The V_{ocp} shows the initial heating of the box followed by thermal equilibration (*ca.* 6,000 seconds), leaving 6,000 seconds (or 60,000 data points) of stable potential difference to give the V_{ocp}.

S6. Exemplar data for temperature profile of air-air apparatus

Temperature monitoring is described in detail in the Experimental section of the manuscript. Below is exemplar data showing *ca.* 19-hour recordings for two thermocells (data point recorded every 0.1 second), with channel 6 = suspended in the centre of the thermostatic heated box; 5 = suspended in the 'hot' air *ca.* 1 mm away from the hot electrode; 4 = immersed in the electrolyte and *ca.* 1 mm away from the hot electrode; 3 = immersed in the electrolyte and *ca.* 1 mm away from the cold electrode; 2 = suspended in the 'cold' air and *ca.* 1 mm away from the hot electrode; and 1 = suspended in the air of the air conditioned laboratory, *ca.* 20 cm away from the heated box and thermocell.

Interestingly, the recorded temperature inside the box (Channels 5 and 6), and inside the electrolyte (Channels 3 and 4) and inside the lab (Channel 1) were all relatively stable. However, the temperature of the air immediately adjacent to the cooler electrode (Channel 2) was slightly higher both at the start of the experiment (up to 15,000 seconds) and near the end of the experiment (70,000 – 77,000 seconds). This corresponded to sunlight directly entering the laboratory window, with experiments starting and finishing in the afternoon, and the cooler period corresponding to dusk, nighttime, and dawn, and as such likely corresponds to some solar irradiation of the black graphite electrode.

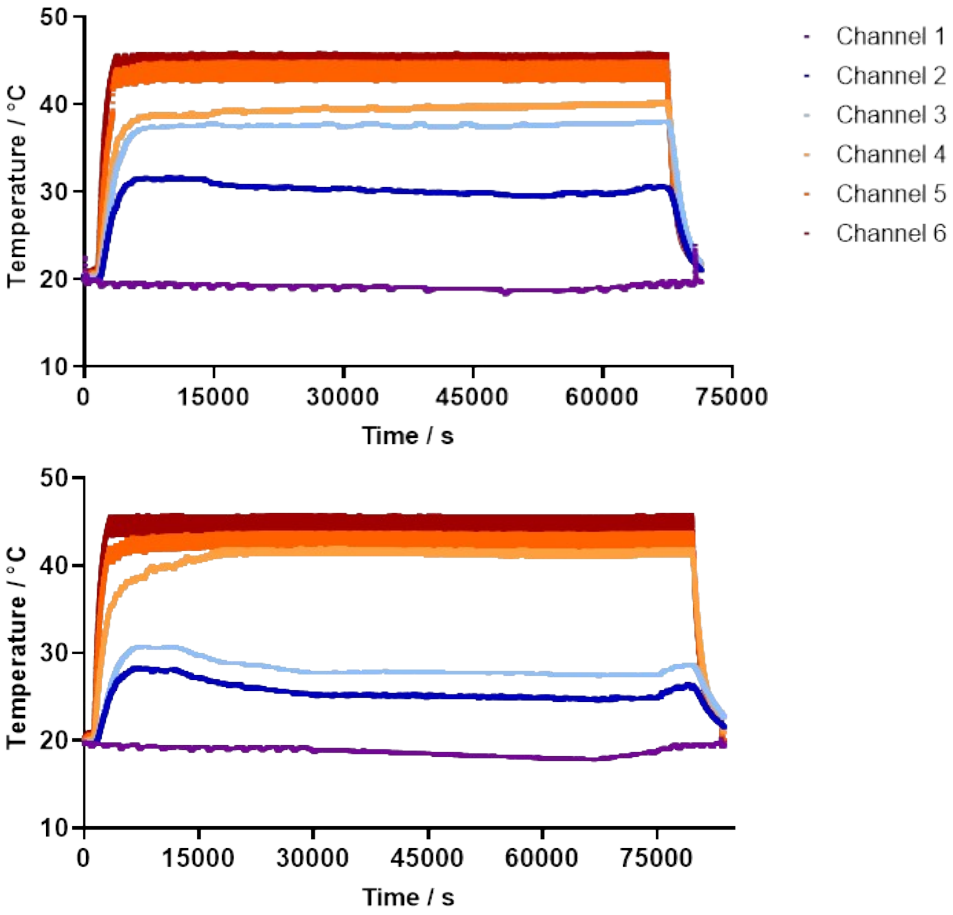

Figure S5. Exemplar data showing the thermistor-recorded temperatures using the air-air setup for (top) 25 mm cell width and (bottom) 100 mm cell width, both containing 0.2 M $K_3[Fe(CN)_6]$, 0.2 M $K_4[Fe(CN)_6]$ and 2.5 wt/v% sodium poyl(acrylate) (and 0.05 M K_2CO_3). A relatively stable temperature difference of 25 ºC was applied. The small gap between channel 3 and 4 values (light blue and light orange, respectively) for 25 mm and large gap for 100 mm is consistent with the V_{ocp} values, *e.g.* large thermocells could sustain a reasonable temperature difference (*ca.* 15 ºC) between the two graphite electrodes, with much of the missing 10 ºC dropped over the colder-side electrode. However, the electrodes in the 25 mm cell experienced only 2 to 3 ºC, with the largest temperature gradient (18 ºC) existing across the colder-side electrode.

S7. Increasing temperature difference experiments in the water-water setup

In order to probe the difference between the 0 wt% system and the 1.5 wt% system as a function of temperature, the applied ΔT was varied. As can be observed in Figure S6 below, the gelled system consistently had a higher V_{ocp}, with the difference increasing as ΔT was increased. This is consistent with the ungelled electrolyte struggling to maintain a stable temperature gradient across the electrodes, which was exacerbated at higher T values due to increased convection. Interestingly the current values were essentially indistinguishable, which suggests any increases in the current due to a higher ΔT value was cancelled out by a commensurate reduction in mass transport. The higher V_{ocp} and equal j_{sc} resulted in higher P_{max} values for the 1.5 wt% system, with the difference also increasing as ΔT was increased

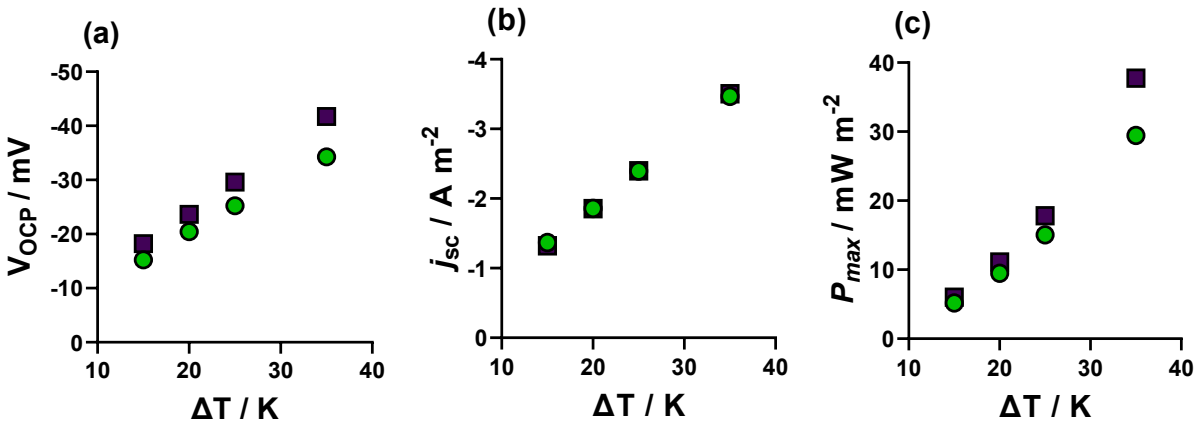

Figure S6. Figure showing the effect of increasing the temperature difference on (a) the liquid, green circles, and (b) 1.5 wt/v% gelled 0.2 M $K_3[Fe(CN)_6]$ and 0.2 M $K_4[Fe(CN)_6]$, purple squares, for the 100 mm cell width thermocell using the liquid-liquid heat exchange set up. The temperature difference was obtained by maintaining the cold electrode (T_{cold}) at 20°C and increasing the hot electrode (T_{hot}) from 35°C (ΔT = 15 K) to 55°C (ΔT = 35 K).

S8. Infra-Red camera observation of the thermocell temperature profile

Figure 3 in the manuscript displays photographs for 0 and 3 wt/v% added sodium poly(acrylate) scenarios; Figure S7 below reproduces these same images here, but also includes the 'optimal' the 1.5 wt/v% scenario. The slurry produced by the added gel material partially reduced heat transfer, enough that a larger ΔT value was experienced at the electrode surfaces. Over time a clear difference between the hot and cold half also clearly formed (centre image).

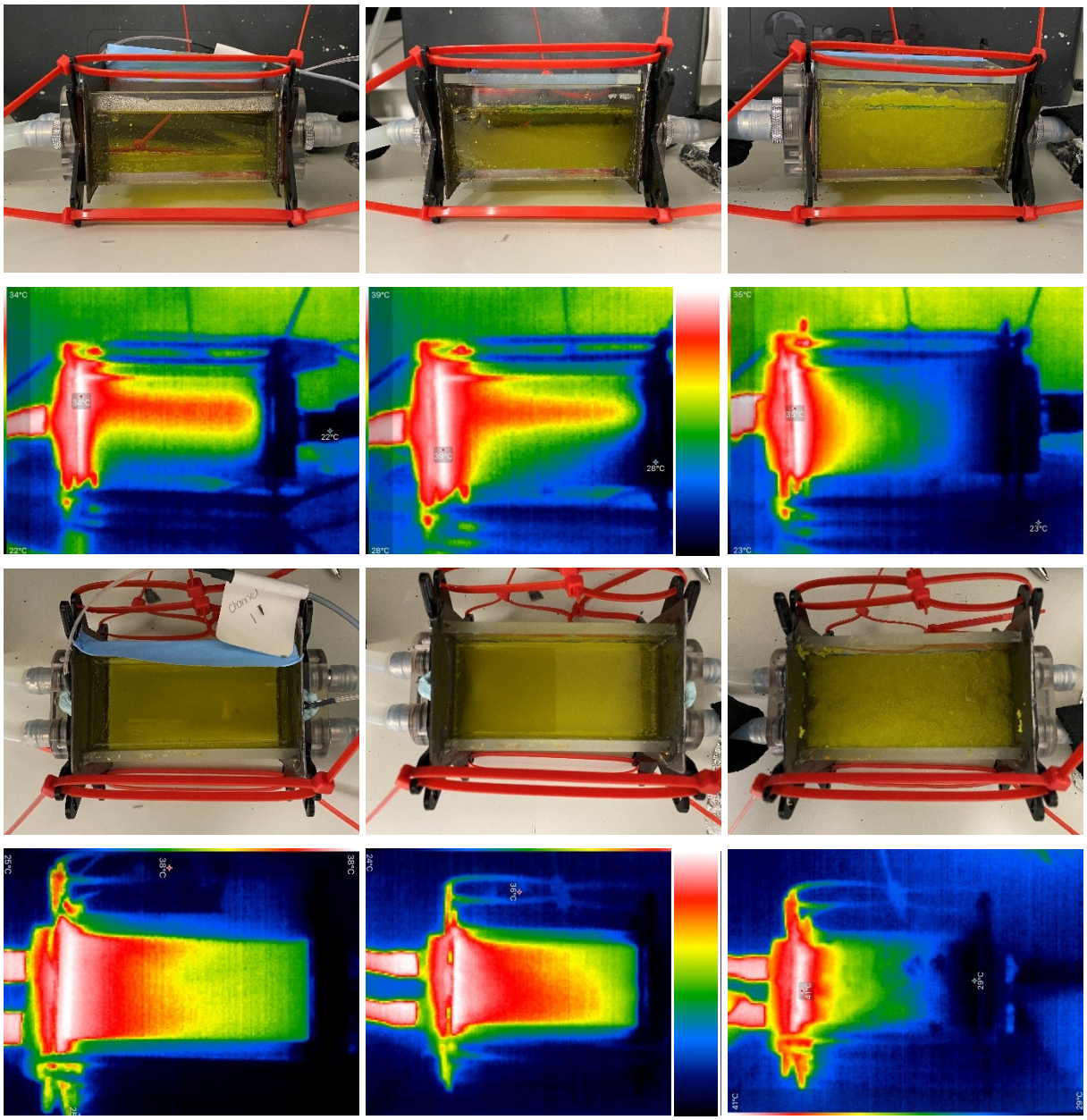

Figure S7. Shows photographs and IR camera images, for (top half) side-on profile and (bottom half) top-down profile of the water-water thermogalvanic cell. The left row has 0 wt%, middle row 1.5 wt% and right row 3 wt% added sodium poly(acrylate). The cells were equilibrated at ΔT = 20 K (T_{cold} =

20°C). The middle row has 2 rainbow-style scale bars; in the IR images the temperature scales are colour-coded going from white (*ca.* 40°C) to dark blue (*ca.* 20°C). Note that the IR images only capture the surface values and not necessarily bulk values. Since the angular emissivity was not calibrated for the wide variety of different surfaces, the values should be taken as semi-quantitative (up to ±5°C). The IR images still accurately highlight relative temperature differences across surfaces composed of the same material.

S9. Tabulated data corresponding to the Figures presented in the manuscript

Table S2: Tabulated values recorded for the 6 thermistors across the 100 mm thermocell as a function on gel wt/v% in the air-air set up (three of these are plotted visually in Figure 3(e)). 0 to 1 mm are taken as the hot electrode; -ve means towards the heater and +ve means towards the colder side, with 101 – 102 mm representing the cold side electrode, and values between 1 and 101 meaning the thermistor is immersed in the gelled electrolyte. The values (-100) and (200) represent the expected ideal temperatures of the heated box and air-conditioned laboratory, respectively. The 'perfect' scenario represents how the hot and cold electrolyte directly adjacent to the electrode are 45 ºC and 20 ºC, respectively. The 'Empty (air only)' scenario represents a sealed 100 mm thermocell but containing only air.

Gel wt/v%	The temperatures recorded by the 6 thermistors / ºC As a function of the distance from the hot electrode / mm where 0 to 1 is the width of this hot electrode							
	(-100)	-6	-1	2	100	103	113	(200)
Perfect scenario	45	45	45	45	20	20	20	20
Empty (air only)	45	45	44.5	43	28	23.7	20	20
0	45	38.9	34.7	30.7	26.3	24.7	21.0	20
0.75	45	42.4	38.6	33.3	28.8	27.8	20.9	20
1.5	45	41.1	39.3	32.8	22.8	23.8	19.7	20
2	45	43.3	42.1	40.5	25.2	23.4	20.8	20
2.5	45	43.9	42.6	42.1	23.9	22.7	20.8	20
3	45	44.4	43.4	38.3	22.3	20.5	19.5	20
3.75	45	44.5	43.5	42.2	25.3	24.0	20.9	20
4.5	45	44.6	44.4	*	*	23.7	20.1	20

* Immersed thermistors malfunctioned during this measurement

Table S3: Tabulated values recorded by immersing thermistors at 50% depth into the 100 mm width thermocell for electrolytes as a function of added sodium poly(acrylate) gelling agent. Thermistors were positioned relative to the hot and cold electrode, with the separation measured using a ruler. A temperature difference, ΔT = 20 K was applied using the water-water setup. The values (-10), (-1), (103) and (110) are assumed to be the applied temperatures, as these refer to the solid copper heat exchanger blocks. Thermistors were held in place until stable temperature values were recorded; since the electrolyte (0 wt/v%) was relatively variable these values are only reported to the nearest ºC.

Added gel / wt/v%	The temperature recorded by the thermistor (ºC) as a function of the distance from the hot electrode (mm) where 0 to 1 is the width of this hot electrode															
	(-10)	(-1)	0.5*	2	3	4	20	40	60	80	98	99	100	101.5*	(103)	(110)
0	40	40	37.5	34	32	30	30	30	30	30	30	27	26	22.5	20	20
1.5	40	40	39.0	37.8	36.4	30.2	29.4	29	26.3	24.7	21.6	20.8	21.0	21.0	20	20
3	40	40	39.75	39.9	**	**	34.1	29	27.4	23.8	**	**	20.4	20.25	20	20

* These values refer to the temperature of the hot electrode (0 to 1 mm) and cold electrode (101 to 102 mm) and are estimated from the ΔT value calculated from the Seebeck coefficient

** Lack of visibility in the opaque gelled mixture meant that these small separations from the electrode could not be accurately located

Table S4: Tabulated values for the data shown in Figure 3 (air-air set-up as a function of wt/v% sodium poly(acrylate) powder for 100 mm width cell). The V_{ocp} and j_{sc} values were measured at an applied ΔT = 25 K, and are the average after *ca.* 40,000 seconds each, with the uncertainty representing 1 standard deviation of this data. The P_{max} value was calculated from $0.25 V_{ocp} j_{sc}$.

Gel / wt/v%	V_{ocp} / mV		j_{sc} / A m^{-2}		P_{max} / mW m^{-2}	
0	-6.27	±0.08	-346.3	±6.3	0.54	±0.02
0.75	-7.97	±0.14	-373.1	±2.7	0.74	±0.02
1.5	-11.36	±0.11	-565.3	±5.5	1.61	±0.03
2	-24.70	±1.00	-684.7	±32.7	4.23	±0.37
2.5	-26.27	±0.52	-791.2	±29.8	5.20	±0.30
3	-28.94	±0.46	-675.0	±23.1	4.88	±0.24
3.75	-25.48	±0.21	-558.6	±7.6	3.56	±0.08
4.5	-27.26	±0.52	-465.6	±9.7	3.17	±0.13

Table S5: Tabulated values for the data shown in Figure 4 (air-air, 2.5 wt/v% gel, hot air convection, cold air stagnant). Measurement conditions and uncertainty as per **Table S4**.

Cell width / mm	V_{ocp} / mV		j_{sc} / A m^{-2}		P_{max} / mW m^{-2}	
25	-12.25	±0.36	-0.61	±0.02	1.87	±0.12
50	-16.62	±0.42	-0.72	±0.02	3.00	±0.18
75	-24.90	±0.11	-0.94	±0.02	5.84	±0.17
100	-26.27	±0.52	-0.79	±0.02	5.20	±0.26

Table S6: Tabulated values for the data shown in Figure 4 (air-air, 2.5 wt/v% gel, both sides with forced convection). Measurement conditions and uncertainty as per **Table S4**.

Cell width / mm	V_{ocp} / mV		j_{sc} / A m^{-2}		P_{max} / mW m^{-2}	
25	-19.41	±0.33	-0.44	±0.01	2.15	±0.08
50	-24.97	±0.38	-1.38	±0.03	8.64	±0.31
75	-29.97	±0.51	-1.33	±0.03	9.98	±0.38
100	-33.21	±0.50	-1.29	±0.03	10.74	±0.39

Supplementary References

1 M. A. Buckingham, S. Hammoud, H. Li, C. J. Beale, J. T. Sengel and L. Aldous, *Sustain. Energy Fuels*, 2020, 4, 3388.

2 P. A. Rock, *J. Phys. Chem.*, 1966, 70, 576–580.

3 M. A. Trosheva, M. A. Buckingham and L. Aldous, *Chem. Sci.*, 2022, 13, 4984–4998.